

# Repulsive Shells

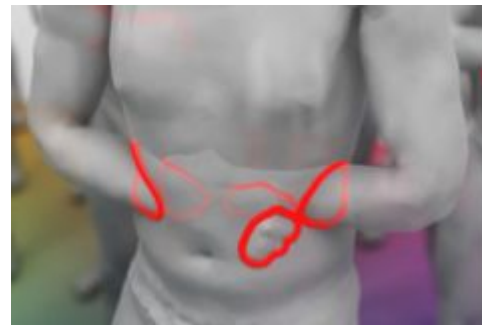
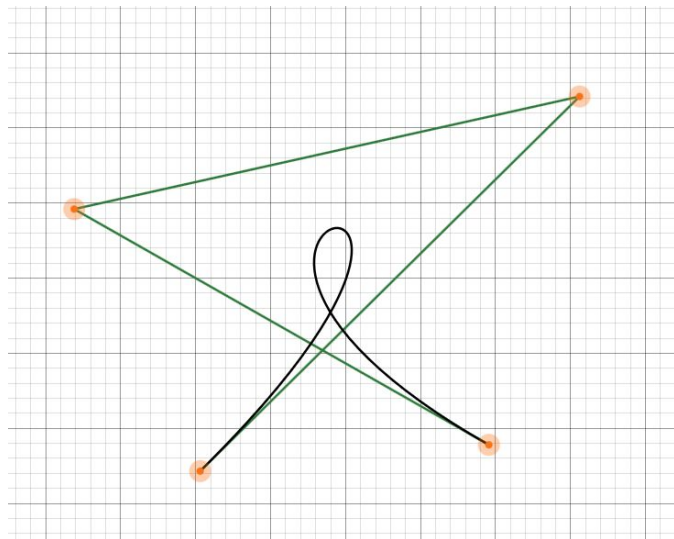
JOSUA SASSEN, HENRIK SCHUMACHER, MARTIN RUMP, KEENAN CRANE

ACM Transactions on Graphics (TOG), Volume 43, Issue 4

SIGGRAPH 2024 Best Paper Award

# Motivation: Intersections/Collisions

- Shape representations permit self-intersections



# Motivation: Intersections/Collisions

- A well-studied subject in physical simulation
  - only tackles detection and resolution of collisions in direct response to local contact
- “In broader geometric computing there are other problems where one must **actively** avoid the influence of self-intersecting states.
  - statistics of nonrigid shapes (e.g., in computational anatomy [Miller et al. 1997])
  - one would like a notion of “average” that yields valid, non-intersecting configurations
  - planning motion trajectories for deformable bodies (e.g., in soft robotics [Fairchild et al. 2021]), one might aim to proactively deform a surface in anticipation of obstacles, rather than reactively slamming on the breaks at the moment of impact.”

Can there be a way to ensure that basic geometric operations are automatically intersection-free?

# Motivating Problem: Averaging Shapes

right arm  
in front



left arm  
in front

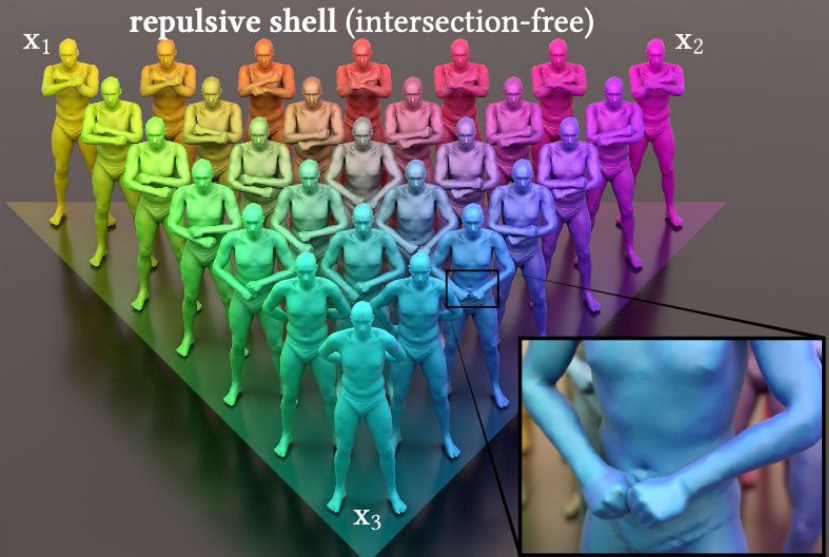
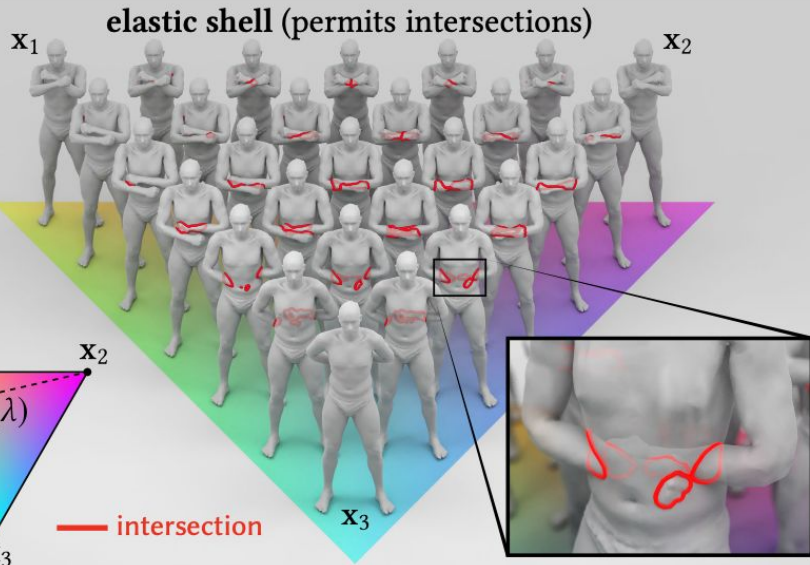


arms  
behind back



Q: What would it mean to take  
the “average” of these poses?





# Motivation: Shape Spaces

- In general, a shape space describes all the different ways a **domain of fixed topology** can be embedded in  $\mathbb{R}^n$ , as well as the **cost of moving around** in this space.

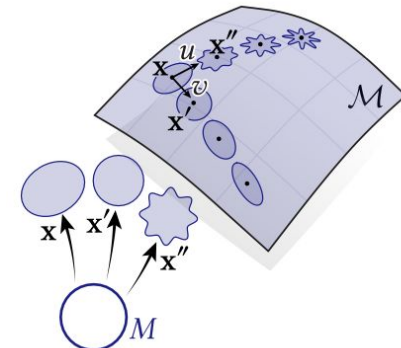


Fig. 5. For a fixed domain  $M$  such as the circle (bottom left), each configuration  $\mathbf{x}: M \rightarrow \mathbb{R}^n$  can be viewed as a point in a shape space  $\mathcal{M}$  (top right). A choice of metric  $g$  on  $\mathcal{M}$  defines the cost of moving from one configuration to another. Here for example we might define  $g$  so that  $\|u\|_g$  is larger than  $\|v\|_g$ .

# Motivation: Shape Spaces

More precisely, for a fixed domain  $M$ , a *configuration manifold*  $\mathcal{M}$  consists of all maps  $\mathbf{x}: M \rightarrow \mathbb{R}^n$  of a certain class, *i.e.*, all ways of assigning a specific geometry to  $M$ . A tangent vector  $u \in T_{\mathbf{x}}\mathcal{M}$  at a point  $\mathbf{x}$  then describes an infinitesimal change to the embedded shape, *i.e.*, a velocity at each point of  $M$  (Figure 5).

A *shape space*  $(\mathcal{M}, g)$  associates a carefully-designed Riemannian metric  $g$  to  $\mathcal{M}$ , which defines the cost of small, infinitesimal deformations. In particular, this metric is a smoothly-varying inner product  $g_{\mathbf{x}}: T_{\mathbf{x}}\mathcal{M} \times T_{\mathbf{x}}\mathcal{M} \rightarrow \mathbb{R}$ . The quantity  $\|u\|_g := \sqrt{g_{\mathbf{x}}(u, u)}$  hence assigns a notion of length to any vector  $u \in T_{\mathbf{x}}\mathcal{M}$ . One can

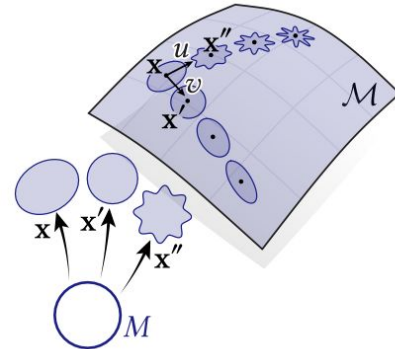


Fig. 5. For a fixed domain  $M$  such as the circle (bottom left), each configuration  $\mathbf{x}: M \rightarrow \mathbb{R}^n$  can be viewed as a point in a shape space  $\mathcal{M}$  (top right). A choice of metric  $g$  on  $\mathcal{M}$  defines the cost of moving from one configuration to another. Here for example we might define  $g$  so that  $\|u\|_g$  is larger than  $\|v\|_g$ .

# Motivation: Shape Spaces

- “One can use this metric to find the shortest interpolating trajectory between two shapes—or perform a number of other tasks (e.g., extrapolation, averaging, or deformation transfer [Heeren et al. 2014]).”

## Exploring the Geometry of the Space of Shells

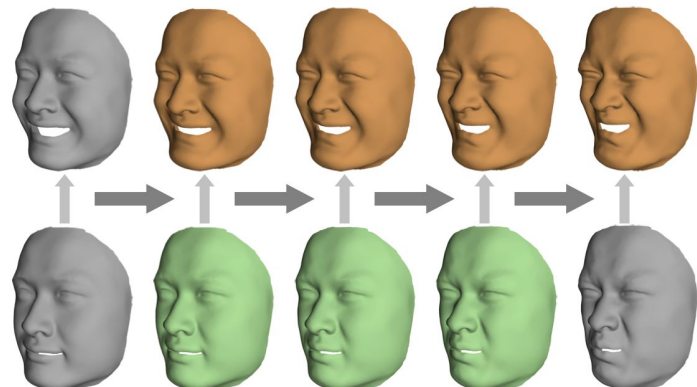
B. Heeren<sup>1</sup>, M. Rumpf<sup>1</sup>, P. Schröder<sup>2</sup>, M. Wardetzky<sup>3</sup> and B. Wirth<sup>4</sup>

<sup>1</sup>Institute for Numerical Simulation, University of Bonn, Germany

<sup>2</sup>Caltech, USA

<sup>3</sup>Institute of Num. and Appl. Math, University of Göttingen, Germany

<sup>4</sup>Institute for Computational and Applied Mathematics, University of Münster, Germany

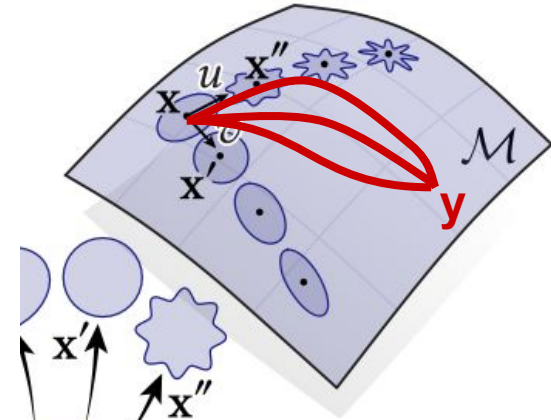


# Motivation: Shape Spaces

tion, averaging, or deformation transfer [Heeren et al. 2014]). For instance, the overall cost of a trajectory  $\mathbf{x}: [0, 1] \rightarrow \mathcal{M}$  can be measured via the *path energy*

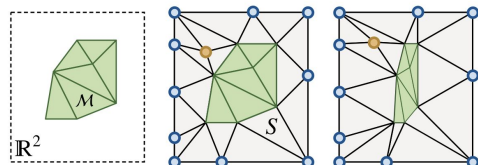
$$\mathcal{E}(\mathbf{x}(t)) := \int_0^1 g_{\mathbf{x}(t)}(\dot{\mathbf{x}}(t), \dot{\mathbf{x}}(t)) dt. \quad (1)$$

The path energy bounds the usual length  $\mathcal{L}(\mathbf{x}(t)) := \int_0^1 \|\dot{\mathbf{x}}(t)\|_g dt$  from above, i.e.,  $\mathcal{L}^2(\mathbf{x}(t)) \leq \mathcal{E}(\mathbf{x}(t))$  for all paths  $\mathbf{x}(t)$ . Critical points of path energy coincide with geodesics that not only locally minimize length, but also have constant speed  $\|\dot{\mathbf{x}}(t)\|_g$  for all  $t$ . The *geodesic distance*  $\text{dist}_g(\mathbf{x}, \mathbf{y})$  gives the *globally* shortest length of any path between  $\mathbf{x}$  and  $\mathbf{y}$ . More explicitly, if  $\mathcal{C}$  is the set of



# Related works: Incorporating Collision Avoidance

- “apply a globally injective deformation to all of space” - depends on space discretization resolution



Simplicial Complex Augmentation Framework for Bijective Maps

ZHONGSHI JIANG, New York University  
SCOTT SCHAEFER, Texas A&M University  
DANIELE PANOZZO, New York University

- “numerical integrators for collision detection and response to broader planning and motion synthesis tasks.” - passive, not time symmetric due to irreversible dynamics

# Related works: Shape Spaces

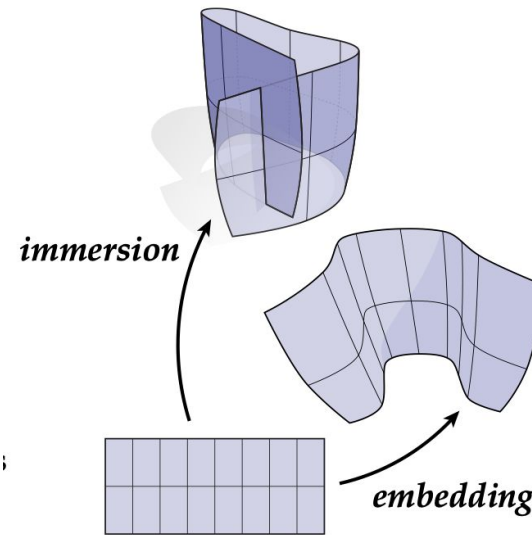
- Some work considers collision-avoiding points on finite-dimensional manifolds, integrating a total repulsive energy over time—but this approach yields undesirable strong artificial expansion



Fig. 3. Simply penalizing the total repulsive potential over a time-varying trajectory yields undesirable deformation: between the fixed start/end configurations, the surface “explodes” away from itself to reduce potential.

# Related works: Shape Spaces

- “Discrete shells” defined by Heeren et al, which this work’s method is based on, consider only immersed rather than embedded surfaces.
- More similar works only consider the space of planar triangular meshes, and do not easily generalize to curved surfaces.



## Related works: Repulsive Potentials

- “Collision Potentials like incremental potential contact (IPC) are unsatisfactory for shape space tasks, as they do not provide sufficient **long-range guidance**.”
- Long-Range Potentials. The basic idea is to mimic the Coulomb potential between electrostatically charged particles  $x$  and  $y$ , i.e.,  $1/(|x - y|^{\alpha})$  for some falloff parameter  $\alpha > 0$ .
  - tangent-point energy (TPE)

## Related works: Repulsive Potentials

- “In the continuous setting, TPE provides an infinite barrier against self-intersection (for surfaces without boundary).”
- For instance, the midpoint TPE scheme of Yu et al. can miss key singularities, whereas IPC does not correspond to a continuous potential.

# Their Approach

- Extending the shape space machinery to incorporate collision avoidance via a **graph manifold construction**.
- A novel **adaptive TPE scheme** which “works on coarse meshes, and converges to a well-defined potential under refinement.”
  - And by applying the fast multipole method, the cost of using TPE is dominated by a small number of near-field interactions.

# Shape Spaces with Collision Avoidance

- “given an existing shape space, how to incorporate collision avoidance?”

A naïve first attempt at avoiding collision is to add a repulsive potential to the path energy  $\mathcal{E}$ , such as the *Coulomb potential*

$$\Phi(\mathbf{x}) := \sum_{i=1}^m \sum_{\substack{j=1 \\ i \neq j}}^m \frac{1}{|x_i - x_j|}. \quad (3)$$

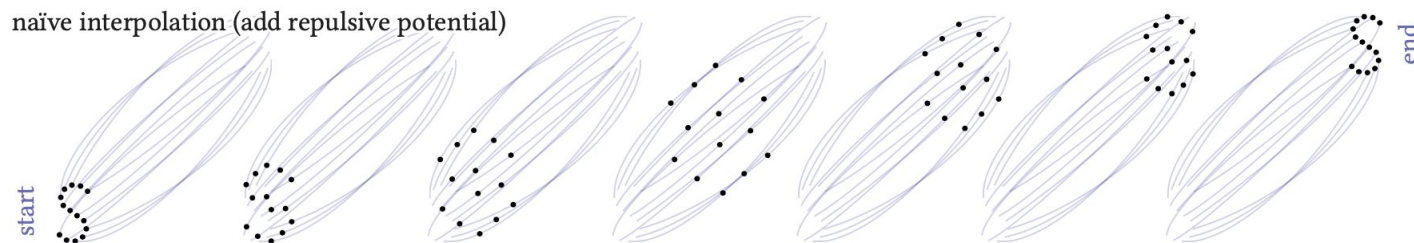
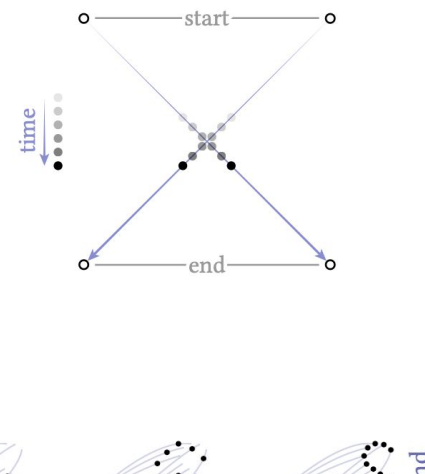
Doing so yields an augmented path energy

$$\tilde{\mathcal{E}}^\Phi(\mathbf{x}) := \int_0^1 g_{\mathbf{x}(t)}(\dot{\mathbf{x}}(t), \dot{\mathbf{x}}(t)) dt + \beta \int_0^1 \Phi(\mathbf{x}(t)) dt, \quad (4)$$

where  $\beta > 0$  is a parameter controlling the strength of repulsion.

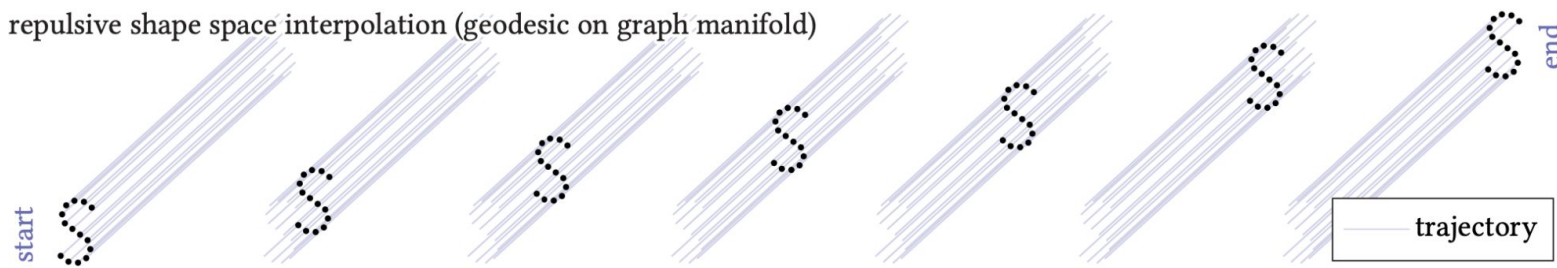
# Shape Spaces with Collision Avoidance

- “Simply minimizing path length yields trajectories that collide”
- “Simply adding a repulsive potential yields a minimizer that expand in the middle of the trajectory

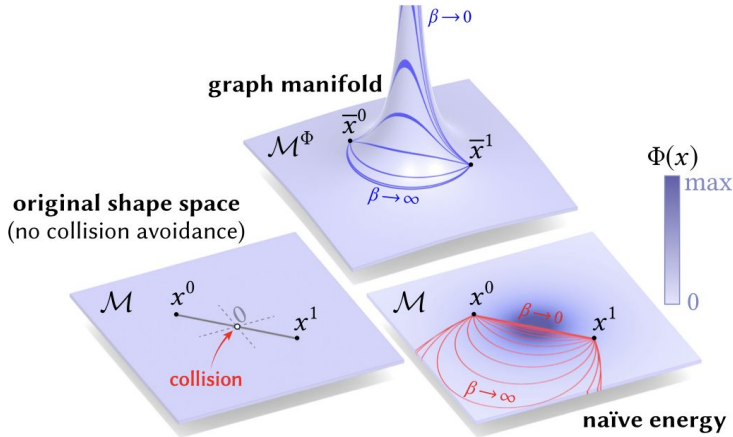


# Graph Manifold

- Key idea: “the change in repulsive potential should be as small as possible throughout the trajectory, while being prohibited from colliding”



# Graph Manifold



colliding. In the Riemannian picture, we use a repulsive potential  $\Phi: \mathcal{M} \rightarrow \overline{\mathbb{R}}$  to define an augmented shape space where configurations naturally avoid collision. In particular, we define what we call a *graph manifold* by appending the potential value  $\Phi(\mathbf{x})$  to each point  $\mathbf{x} \in \mathcal{M}$ , effectively embedding our original shape space in a space one dimension higher:

$$\mathcal{M}^\Phi := \{(\mathbf{x}, \Phi(\mathbf{x})) \mid \mathbf{x} \in \mathcal{M}\} \subset \mathcal{M} \times \overline{\mathbb{R}}.$$

Intuitively, configurations with collisions now correspond to “infinitely tall mountains” that we do not wish to climb (e.g., Figure 8, top).

Velocities are in turn vectors tangent to this mountain range—in particular, the tangent spaces of the graph manifold are given by

$$T_{(\mathbf{x}, \Phi(\mathbf{x}))} \mathcal{M}^\Phi = \{(u, d_{\mathbf{x}}\Phi(u)) \mid u \in T_{\mathbf{x}}\mathcal{M}\},$$

where at each point  $\mathbf{x} \in \mathcal{M}$  the directional derivative  $d_{\mathbf{x}}\Phi(u)$  describes the change in potential  $\Phi$  due to a infinitesimal motion  $u$  along the original shape space. We define the metric on  $\mathcal{M}^\Phi$  as

$$\overline{g}_{(\mathbf{x}, \Phi(\mathbf{x}))}^\Phi ((u, s), (v, t)) := g_{\mathbf{x}}(u, v) + \beta s t,$$

for  $(u, s), (v, t) \in T_{(\mathbf{x}, \Phi(\mathbf{x}))} \mathcal{M}^\Phi$  where  $\beta$  controls the strength of repulsion (as in Equation 4). We can also express this metric with respect to the original configuration space  $\mathcal{M}$ , namely

$$g_{\mathbf{x}}^\Phi(u, v) := g_{\mathbf{x}}(u, v) + \beta d_{\mathbf{x}}\Phi(u) d_{\mathbf{x}}\Phi(v). \quad (5)$$

# Graph Manifold

- Geodesic paths hence try to maintain a roughly constant repulsive potential, while still keeping as straight as possible with respect to the original metric  $g$

To see this, denote by  $\mathcal{C}$  the set of continuously differentiable curves  $c: [0, 1] \rightarrow \mathcal{M}$  satisfying  $c(0) = x$  and  $c(1) = y$ . We use the definition of the Riemannian distance and see

$$\begin{aligned}\text{dist}_\Phi(x, y) &:= \inf_{c \in \mathcal{C}} \int_0^1 \sqrt{g(\dot{c}(t), \dot{c}(t)) + (d_{c(t)}\Phi \dot{c}(t))^2} dt \\ &\geq \inf_{c \in \mathcal{C}} \int_0^1 \sqrt{(d_{c(t)}\Phi \dot{c}(t))^2} dt \\ &= \inf_{c \in \mathcal{C}} \int_0^1 |d_{c(t)}\Phi \dot{c}(t)| dt \geq |\Phi(y) - \Phi(x)|.\end{aligned}$$

From the last estimate, it immediately follows that  $\text{dist}_{g^\Phi}(x, y) = \infty$  if  $\Phi(y) = \infty$ . In other words, beyond merely ensuring that invalid states  $x$  have infinite energy, we have made certain that geodesic paths in our repulsive shape space cannot reach invalid states in

# Surface Energies: Shell Energy

- A thin shell is, roughly speaking, a solid object with very small thickness  $\delta > 0$ , dominated by elastic behavior: it always tries to restore a deformed shape to some fixed reference configuration.

$$\mathcal{W}(\mathbf{x}, \tilde{\mathbf{x}}) := \mathcal{W}_{\text{membrane}}(\mathbf{x}, \tilde{\mathbf{x}}) + \mathcal{W}_{\text{bending}}(\mathbf{x}, \tilde{\mathbf{x}}),$$

# Surface Energies: Shell Energy

*Smooth.* A *membrane energy* accounts for tangential stretching and shearing of the surface, and in our case is given by

$$\mathcal{W}_{\text{membrane}}(\mathbf{x}, \tilde{\mathbf{x}}) := \delta \int_M W(\mathbf{I}^{-1}\tilde{\mathbf{I}}) dA, \quad (9)$$

where  $\mathbf{I} := \mathbf{J}_x^T \mathbf{J}_x$  is the metric or *first fundamental form* induced by  $\mathbf{x}$  (and likewise for  $\tilde{\mathbf{I}}$ ). The quantity  $\mathbf{I}^{-1}\tilde{\mathbf{I}}$  is called the *Cauchy–Green strain tensor*, and encodes the change of metric due to the deformation. The function  $W$  describes the stress-strain response of the material—we use the *neo-Hookean energy density*

$$W(A) := \frac{\mu}{2} \operatorname{tr} A + \frac{\lambda}{4} \det A - \left( \frac{\mu}{2} + \frac{\lambda}{4} \right) \log(\det A) - \mu - \frac{\lambda}{4}. \quad (10)$$

Here  $\lambda$  and  $\mu$  are positive material constants (called the *first and second Lamé parameters, resp.*).

*Smooth.* A *bending energy* accounts for bending of the surface in the normal direction. We use the energy

$$\mathcal{W}_{\text{bending}}(\mathbf{x}, \tilde{\mathbf{x}}) := \delta^3 \int_M \|\tilde{\mathbf{II}} - \mathbf{II}\|_F^2 dA, \quad (12)$$

where  $\|\cdot\|_F$  is the Frobenius norm, and  $\mathbf{II}$  is the *second fundamental form*, given by  $\mathbf{II}(X, Y) := \langle d\mathbf{x}(X), d\mathbf{n}(Y) \rangle$  for all tangent vectors  $X, Y$  (and likewise for  $\tilde{\mathbf{II}}$ ). Intuitively, this energy penalizes a change in curvature along any direction.

# Surface Energies: Shell Energy

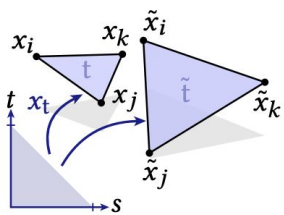
(Discretize)

*Discrete.* A triangle  $t \in T$  with vertices  $i, j, k \in V$  is embedded in  $\mathbb{R}^3$  via the map  $x_t(s, t) := x_i + s(x_j - x_i) + t(x_k - x_i)$  on the standard triangle  $\{(s, t) \in \mathbb{R}_{\geq 0}^2 | s + t \leq 1\}$  (see inset). Hence, the metric is constant in each triangle, given by  $I_t := J_t^T J_t$ , with

$$J_t := \begin{bmatrix} x_j - x_i & x_k - x_i \end{bmatrix} \in \mathbb{R}^{3 \times 2},$$

and likewise for  $\tilde{J}_t$  (where each  $x_i \in \mathbb{R}^3$  is viewed as a column vector). The energy in Equation 9 can then be discretized via the sum

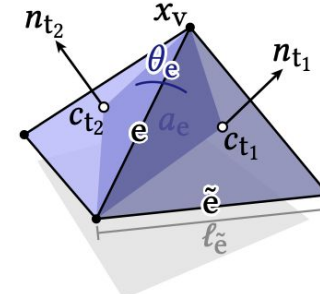
$$\widehat{\mathcal{W}}_{\text{membrane}}(\mathbf{x}, \tilde{\mathbf{x}}) = \delta \sum_{t \in T} a_t W(I_t^{-1} \tilde{I}_t). \quad (11)$$



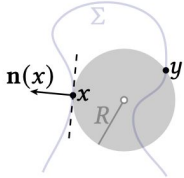
*Discrete.* For a triangle mesh, we use the discrete bending energy

$$\widehat{\mathcal{W}}_{\text{bending}}(\mathbf{x}, \tilde{\mathbf{x}}) = \delta^3 \sum_{e \in E_{\text{int}}} (2 \tan(\tilde{\theta}_e/2) - 2 \tan(\theta_e/2))^2 \ell_e^2 / a_e,$$

where we have applied a standard discretization of normal curvature [Crane and Wardetzky 2017]. Similar to the logarithm in the membrane energy, the use of the tan function prevents foldovers (*i.e.*,  $\theta_e = \pi$ ). In practice, most dihedral angles are small, and we find it



# Surface Energies: Repulsive Energy



**3.2.1 Tangent-Point Energy (Smooth).** Let  $\Sigma := \mathbf{x}(M) \subset \mathbb{R}^3$  denote the embedded surface. For any two points  $x, y \in \Sigma$  the *tangent-point radius*  $R(x, y)$  is defined as the radius of the smallest sphere through  $x$  and  $y$  that is tangent to  $\Sigma$  at  $x$ . This radius can be expressed as

$$R(x, y) := \frac{|x - y|^2}{2 |\langle \mathbf{n}(x), x - y \rangle|},$$

where  $\mathbf{n}(x)$  is the unit normal at  $x$ . The *tangent-point energy* is then

$$\Phi(\mathbf{x}) := \int_{\Sigma} \int_{\Sigma} \frac{|\langle \mathbf{n}(x), x - y \rangle|^{\alpha}}{|x - y|^{2\alpha}} dx dy, \quad (13)$$

where  $\alpha \geq 1$  is a parameter that controls the strength of repulsion.

For surfaces without boundary, this energy is finite if and only if (i) the surface has no self-intersections, and (ii)  $\mathbf{x}$  is sufficiently regular [Strzelecki and von der Mosel 2013; Blatt 2013]. In particular, polyhedral surfaces (which are only  $C^0$ ) will have infinite energy: normals do not become parallel as points approach opposite sides of an edge. Hence, the numerator does not approach zero, as it would for a smoother surface. We must hence be careful when defining our

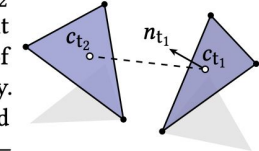
**3.2.2 Tangent-Point Energy (Discrete).** Yu et al. [2021a] discretize tangent-point energy by applying midpoint quadrature to Equation 13 for each triangle pair, yielding the expression

$$\widehat{\Phi}(\mathbf{x}) := \sum_{t_1 \in T} \sum_{t_2 \in T} \sum_{t_1 \neq t_2} a_{t_1} a_{t_2} K(c_{t_1}, c_{t_2}, \mathbf{n}_{t_1}), \quad (14)$$

where  $k$  is the discrete tangent-point kernel

$$K(x, y, n) := \frac{|\langle n, x - y \rangle|^{\alpha}}{|x - y|^{2\alpha}}. \quad (15)$$

Omitting the summand for  $t_1 = t_2$  (which would be undefined) is consistent with the fact that every planar piece of a surface has zero tangent-point energy. Moreover, since we evaluate the integrand only at midpoints—and not near edges—the fact that the surface is only  $C^0$  does not cause the energy to blow up in this case. Consistency of this discretization has been verified experimentally by Yu et al. [2021a, Section 8.1]. However, several challenges remain, as will be discussed in Section 5.

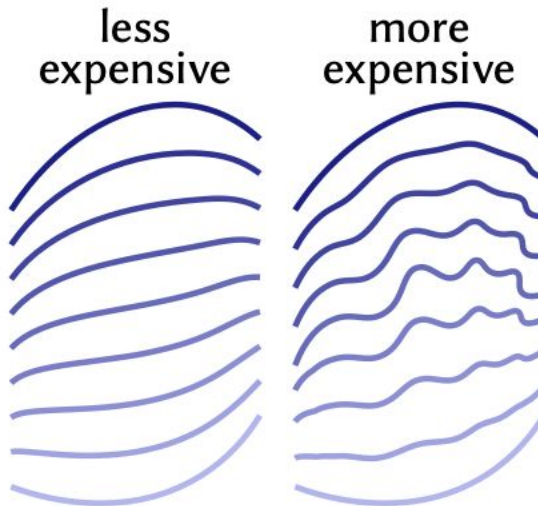


# Elastic Shells

From a geometric perspective, strain rates correspond to tangent vectors  $u \in T_x \mathcal{M}$ . To penalize dissipation we hence define the elastic metric  $g$  as

$$g_x(u, v) := \frac{1}{2} d_y^2 \mathcal{W}(x, y) \Big|_{y=x} (u, v), \quad (16)$$

since the Hessian  $d_y^2 \mathcal{W}$  provides a local quadratic model of the energy  $\mathcal{W}$ . Moreover, since  $y = x$  is always a minimizer of this energy,



# Repulsive Shells

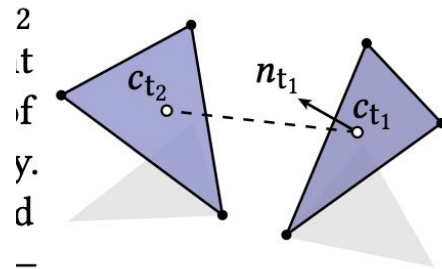
## Graph Manifold of Elastic Shells + TPE

havior. Instead, we define our repulsive shape space as the manifold  $(\mathcal{M}, g^\Phi)$  where

- the configuration space  $\mathcal{M}$  is the collection of  $C^2$  embeddings  $\mathbf{x}: M \rightarrow \mathcal{M}$  of a surface  $M$ ,
- the metric  $g$  on  $\mathcal{M}$  is the shell metric from Equation 16, and
- the potential  $\Phi$  used to construct the graph manifold is the tangent-point energy given in Equation 13.

# Adaptive TPE

- The discrete TPE energy mentioned earlier still allows self intersections
- The authors apply a hierarchical fast multipole method to refine interactions between nearby elements.



# Adaptive TPE

- Each node also stores the total area  $a$ , center of mass  $c$ , and area-weighted average normal  $n_U$
- “Block cluster tree. The BVH in turn defines a block cluster tree (BCT) that can be used to approximate the energy and its differential.

*Bounding volume hierarchy.* We start by building a standard *bounding volume hierarchy (BVH)* for the mesh, i.e., a binary tree where triangles of  $\Sigma_h$  are hierarchically clustered into *axis-aligned bounding boxes (AABBs)* [Yu et al. 2021a, Section 4]. We will use  $U_1, U_2$  to denote the two children of any BVH node  $U$ . Each node also stores the total area  $a_U$ , center of mass  $c_U$ , and area-weighted average normal  $n_U$  of all the triangles it contains. In particular, for each node  $U$  we compute

$$a_U = a_{U_1} + a_{U_2}, \quad c_U = \frac{a_{U_1}c_{U_1} + a_{U_2}c_{U_2}}{a_U}, \quad n_U = \frac{a_{U_1}n_{U_1} + a_{U_2}n_{U_2}}{a_U}. \quad (21)$$

In particular, each node of the BCT is a pair  $(U, V)$  of nodes from the BVH, with children  $(U_1, V_1), (U_1, V_2), (U_2, V_1), (U_2, V_2)$ , starting with the root node  $(\Sigma_h, \Sigma_h)$ .

# Adaptive TPE

- Multipole Acceptance Criterion (MAC)

TPE considers whether two surface patches  $U_1, U_2 \subset \Sigma$  are small relative to the distance between them. In particular, if  $\text{diam}(U)$  is the greatest distance between any two points in  $U$  and  $\text{conv}(U)$  is its convex hull, then our MAC is

$$\max \{\text{diam}(U_1), \text{diam}(U_2)\} \leq \theta \text{dist}(\text{conv}(U_1), \text{conv}(U_2)), \quad (18)$$

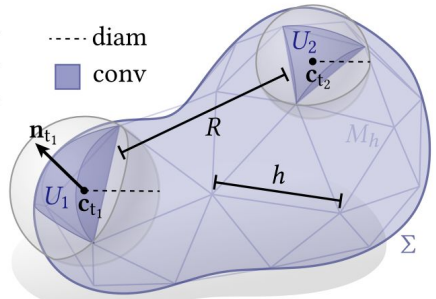
where  $\text{dist}(A, B)$  is the smallest distance between any two points  $a \in A, b \in B$ . The parameter  $\theta > 0$  controls how aggressively we replace exact patch interactions with a simpler proxy—and hence the accuracy of our approximation. In particular, if we replace each patch  $U$  with its center of mass  $c(U)$  and average normal  $\bar{n}(U)$ , then we get a multipole approximation of the TPE restricted to these surfaces patches  $\Phi(U_1, U_2)$  with error of order  $O(\theta^2)$ :

$$\Phi(U_1, U_2) = \text{area}(U_1) \text{area}(U_2) \frac{|\langle \bar{n}(U_1), c(U_1) - c(U_2) \rangle|^\alpha}{|c(U_1) - c(U_2)|^{2\alpha}} + O(\theta^2). \quad (19)$$

In practice, we cannot evaluate the multipole approximation directly, because we have only a triangulation and not the smooth surface  $\Sigma$ . Suppose, however, that  $\Sigma_h$  is a *closely inscribed* triangle mesh (in the sense of Morvan and Thibert [2002]) with maximum edge length  $h$ . Consider then two triangles  $t_1, t_2$  in  $\Sigma_h$ , and the two corresponding surface patches  $U_1, U_2 \subset \mathbb{R}^3$  obtained by closest-point projection onto  $\Sigma$  (see inset). Since the triangle normal  $n_{t_1}$  approximates  $\bar{n}(U_1)$  up to  $O(h)$  [Morvan and Thibert 2002], we get

$$\Phi(U_1, U_2) = a_{t_1} a_{t_2} \frac{|\langle n_{t_1}, c_{t_1} - c_{t_2} \rangle|^\alpha}{|c_{t_1} - c_{t_2}|^{2\alpha}} + O(h + \theta^2). \quad (20)$$

Hence, as long as we pick  $\theta^2 \in O(h)$  and satisfy the MAC for this  $\theta$  value, our discrete energy  $\widehat{\Phi}(\Sigma_h)$  will approximate the continuous energy  $\Phi(\Sigma)$  up to an additive error of size at most linear in  $h$ . This calculation agrees with experiments by Yu et al. [2021a, Section 8.1].



# Adaptive TPE

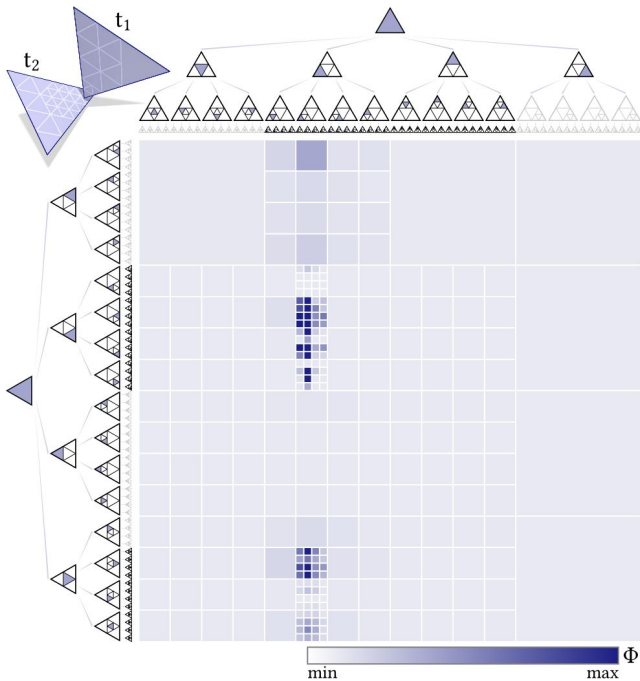


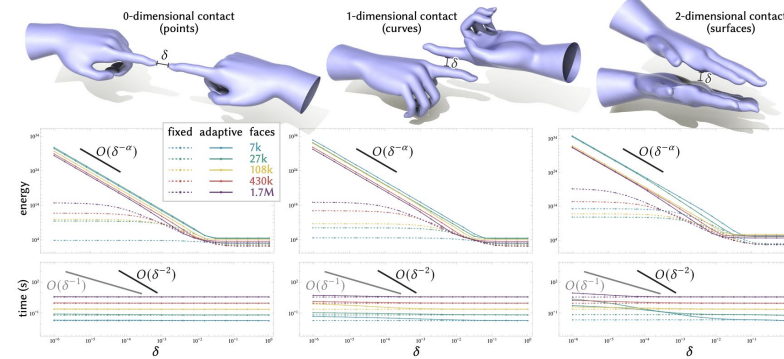
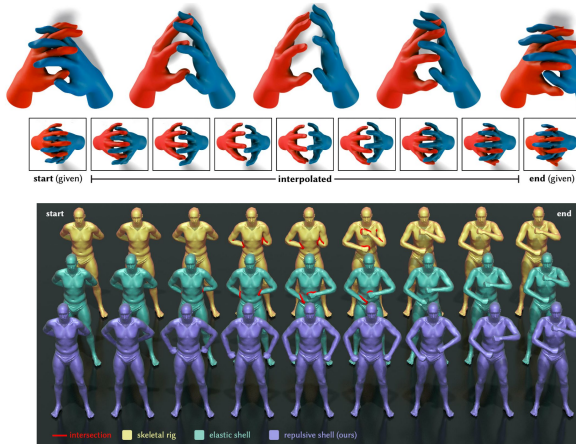
Fig. 13. When two triangles  $t_1, t_2$  are in near-contact, it may be insufficient to approximate the repulsive energy using just their centers. Instead, we pretend that each triangle has been subdivided hierarchically into infinitely many pieces, and continue running the usual multipole approximation algorithm. Here we show the sub-trees implicitly used for approximation; each block corresponds to an energy term in our sum. Note however that we do not explicitly build these trees.

# Examples



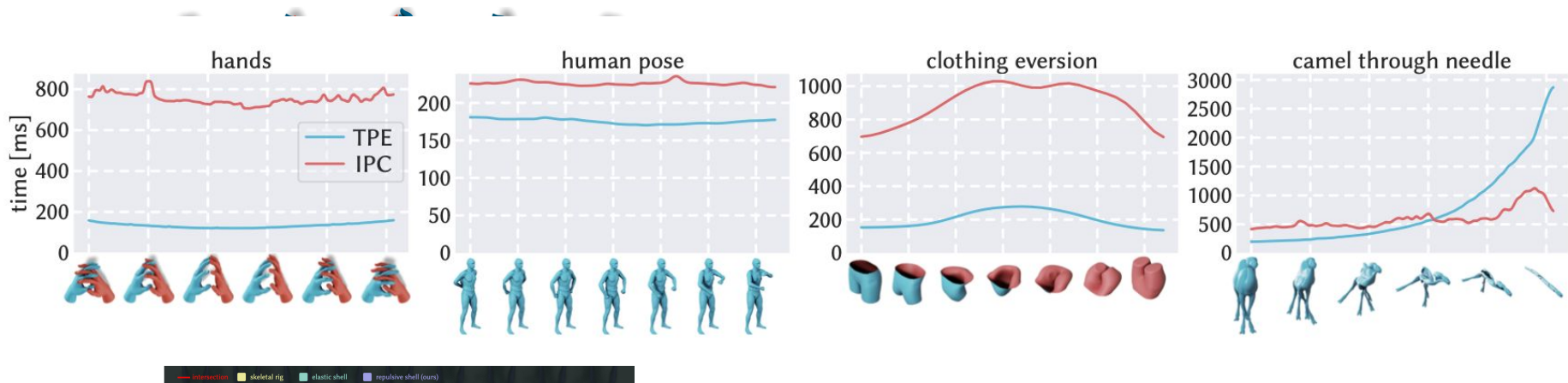
# Evaluations

- “ Most experiments were run on a Intel i7 1260p laptop with 4 performance cores and 32GB RAM; to generate final 60fps frame rate animation we used a single workstation with two 32-core AMD EPYC 7601 processors with 1TB RAM”



# Evaluations

- “ Most experiments were run on a Intel i7 1260p laptop with 4 performance cores and 32GB RAM; to generate final 60fps frame rate animation we used a single workstation with two 32-core AMD EPYC 7601 processors with 1TB RAM”



# Limitations

- Surfaces with Boundary.
- Numerics.
- Alternative Potentials.
- Not Realtime
- Scalability
- Fixed Topology Assumption

# Conclusion

- The authors proposed a shape space frame work where geometric operations done on it are ensured to be intersection free.
- The authors also came up with a algorithm for calculating the discrete tangent point energy on a triangle mesh that works on coarse meshes, and converges to a well-defined potential under refinement.